

# Monitoring rock desert formation caused by two different origins (ice-snow melting and drying) in the Qinghai-Tibet Plateau of China by considering topographic and meteorological elements

JIA Wei<sup>1,2</sup>, SHI Peijun<sup>3,4\*</sup>, WANG Jing'ai<sup>1,4,5</sup>, MA Weidong<sup>2</sup>, XIA Xingsheng<sup>2,3</sup>, ZHOU Yuantao<sup>2</sup>

<sup>1</sup> Key Laboratory of Tibetan Plateau Land Surface Processes and Ecological Conservation (Ministry of Education), Qinghai Normal University, Xining 810008, China;

<sup>2</sup> School of Geographical Sciences, Qinghai Normal University, Xining 810008, China;

<sup>3</sup> Academy of Plateau Science and Sustainability, Qinghai Normal University, Xining 810008, China;

<sup>4</sup> Key Laboratory of Environmental Change and Natural Disaster, Ministry of Education, Beijing Normal University, Beijing 100875, China;

<sup>5</sup> Faculty of Geographical Science, Beijing Normal University, Beijing 100875, China

**Abstract:** Monitoring rock desert formation caused by two different origins (ice-snow melting and drying) through remote sensing is crucial to our understanding of the interaction between the underlying surface of different rock desert and land-atmosphere types, as well as the relationship between bare land and soil erosion. A number of achievements have been made in remote sensing monitoring of desert areas, but there is a lack of accurate classification and remote sensing identification of rock desert types based on formation mechanism. In this study, the north and south sides of the eastern Kunlun Mountains in the northern part of the Qinghai-Tibet Plateau of China were taken as the study areas. Landsat operational landscape imager, digital elevation model, and precipitation and temperature grid data were used as data sources. By identifying the bare areas based on the normalized difference vegetation index (NDVI), we used the multi-element fusion method of contours, isotherms, and isohyets to identify the rock desert types in the ice-snow melting and dry areas. The results showed that: (1) the rock desert areas identified by remote sensing based on topographic and meteorological elements were highly accurate, with an overall accuracy of 88.45% and kappa coefficient of 0.77. The multi-element fusion method of contours, isotherms, and isohyets could effectively identify the rock desert types in the ice-snow melting and dry areas; (2) the optimal segmentation range of the ice-snow melting and dry areas was 3600 m contour,  $-2^{\circ}\text{C}$ – $2^{\circ}\text{C}$  isotherms, and 100–130 mm isohyets. The areas with elevation less than 3600 m, annual average temperature higher than  $2^{\circ}\text{C}$ , and average annual precipitation less than 100 mm were rock desert in the dry areas. The range of  $-2^{\circ}\text{C}$ – $2^{\circ}\text{C}$  isotherms and 100–130 mm isohyets was the transition area between the ice-snow melting and dry areas. The areas with elevation higher than 3600 m, annual average temperature less than  $-2^{\circ}\text{C}$ , and average annual precipitation higher than 130 mm were rock desert in the ice-snow melting areas; and (3) the identification accuracy of the bare areas based on the NDVI method was better, specifically, the identification accuracy of plain bare areas was generally better than that of mountain bare areas. The remote sensing identification method considers not only the topographic factors that have great influence on the spatial distribution of the two types of rock desert areas, but also the meteorological factors, which can provide a scientific reference for the effective identification of the two types of rock desert areas.

\*Corresponding author: SHI Peijun (E-mail: [spj@bnu.edu.cn](mailto:spj@bnu.edu.cn))

Received 2022-05-14; revised 2022-06-26; accepted 2022-07-15

© Xinjiang Institute of Ecology and Geography, Chinese Academy of Sciences, Science Press and Springer-Verlag GmbH Germany, part of Springer Nature 2022

**Keywords:** rock desert in the ice-snow melting areas; rock desert in the dry areas; contours; isotherms; isohyets; Qinghai-Tibet Plateau

**Citation:** JIA Wei, SHI Peijun, WANG Jing'ai, MA Weidong, XIA Xingsheng, ZHOU Yuantao. 2022. Monitoring rock desert formation caused by two different origins (ice-snow melting and drying) in the Qinghai-Tibet Plateau of China by considering topographic and meteorological elements. *Journal of Arid Land*, 14(8): 849–866. <https://doi.org/10.1007/s40333-022-0100-2>

## 1 Introduction

A rock desert is a geographical landscape with sparse or bare surface vegetation formed under drought or alpine climate conditions (UNCCD, UNDP, 2012; Zhang et al., 2019), which affects the production and livelihood of over 110 countries and regions worldwide, especially in arid areas (Han et al., 2021). Since the 1990s, the environmental and social problems caused by rock desertification have become one of the key factors hindering the sustainable development of arid, semi-arid, and sub-humid areas, which account for 41% of the global land area (Hendersonsellers, 1996; Li et al., 2016). The land surface matter controls the distribution of water and energy flux, while the expansion of rock desert changes the properties of the underlying surface. Changes of underlying surface properties are accompanied by those of landing surface parameters, which are fed back to the atmosphere through energy distribution, and in turn affect the near-surface climate. Near-surface temperature is particularly sensitive to these changes, affecting not only atmospheric circulation, but also regional and global climate (Li et al., 2015; Gevaert et al., 2017).

The Qinghai-Tibet Plateau, located more than 4000 m above sea level (a.s.l.), is the largest and highest plateau in the world. It is also known as the "Third Pole" and the "Roof of the World" (Kang et al., 2019; Yang et al., 2019; Yao et al., 2019). The Qinghai-Tibet Plateau has long been considered as one of the most sensitive regions to global climate change (Chang et al., 2017; Zhang et al., 2018). Through the combination of summer monsoon, winter monsoon, and mid-latitude westerly wind, a cold and dry continental climate prevails on the Qinghai-Tibet Plateau (Böhner, 2006; Stauch, 2015). The strong winter wind causes frequent frost weathering and strong wind erosion, which promotes the formation of sandy materials on the plateau (Li et al., 2016). Therefore, the unique geographical location, strong wind, abundant sand sources, and cold and dry climate are all favorable conditions for the occurrence of plateau rock desert (Zhang et al., 2012; Hu et al., 2015). At present, the existing and potential desertification land on the Qinghai-Tibet Plateau is approximately  $3.93 \times 10^5 \text{ km}^2$  (accounting for 15.10% of the total land area of the plateau) and  $2.99 \times 10^4 \text{ km}^2$ , respectively, (Li et al., 2018). The northern part of the plateau is the national key desertification areas, primarily distributed in the Qaidam, Gonghe, and Qinghai Lake basins and the Three-River Headwaters Region on the Qinghai-Tibet Plateau (Hua et al., 2012). Furthermore, the process of rock desert on plateau land is gradually intensifying (Xie et al., 2013; Zu et al., 2014).

Remote sensing is an important tool for monitoring and evaluating rock desert (Kefi et al., 2007; Miao et al., 2015), which can provide high-precision data covering a wide range of observations (Hu et al., 2020). In recent decades, many scholars at home and abroad have monitored desertification in Qinghai-Tibet Plateau through remote sensing (Yan et al., 2009; Li et al., 2016; Zhang et al., 2018; Sun et al., 2019). The existing remote sensing monitoring of desertification primarily includes index extraction methods based on the normalized difference vegetation index (NDVI) and image classification methods (visual interpretation and computer automatic classification methods) (Dawelbait et al., 2012; Higginbottom et al., 2014; Lamchin et al., 2016; Guo et al., 2021; Jia et al., 2021), these remote sensing methods provide scientific and effective support for monitoring desertification and dynamic change. At present, most studies focus on remote sensing monitoring of plateau desertification from the degree of desertification, but lack of accurate classification and remote sensing identification of the rock desert types in the

Qinghai-Tibet Plateau based on the formation mechanism.

The surface matter of different rock desert types controls the distribution of energy flux and water and plays a vital role in the climate system. The interaction between the surface matter and atmosphere is an important driving factor of climate (Gevaert et al., 2017). The exchange of energy, momentum, and matter between the atmosphere and surface is the key to the land-atmosphere interaction, which affects the local and regional atmospheric circulation and climate change. The land-atmosphere interaction plays a significant role in regional and global land physical processes, atmospheric circulation, and climate change (Liu et al., 2011). There are various types of soil erosion in the Qinghai-Tibet Plateau. In the ice-snow melting areas, the rock desert formed through the combined action of freeze-thaw, gravity, wind, and fluvial erosion can be called rock desert in the ice-snow melting areas. In the dry areas, the rock desert formed by the wind erosion of drying denudation can be called rock desert in the dry areas. Rock desert in both the ice-snow melting and dry areas is the product of climate change, but the soil erosion dynamics of these two types of rock desert are completely different, and the underlying surface types are also different. For the rock desert in the ice-snow melting areas, with the warming of climate and the retreat of snow line, the exposed bedrock continues to increase, and the particle size of surface weathering becomes smaller due to multiple dynamic erosion. However, the rock desert in the dry areas is a bare land dominated by precipitation stress, with large landscape gradient, poor soil and water conservation ability, and low soil fertility. With wind erosion, the particle size and spatial distribution of rock desert also change. Their spatial distribution of the two types of rock desert is directly related to elevation, temperature, and precipitation. Therefore, it is important to recognize the interaction between bare land and soil erosion, as well as the relationship between the underlying surface of different rock desert and land-atmosphere types, for identifying the rock desert in the ice-snow melting and dry areas by remote sensing based on the comprehensive topographic and meteorological factors.

In this study, the Yuzhu Peak region located in the eastern area of Kunlun Mountains in the northern Qinghai-Tibet Plateau is selected as the sampling area. We used the 2020 Landsat8 operational landscape imager (OLI) remote sensing data as the data source, and the digital elevation model (DEM) and meteorological raster data as the auxiliary data. According to the description of the formation mechanism, material composition, and spatial distribution of rock desert in the ice-snow melting and dry areas of the Qinghai-Tibet Plateau, we constructed the optimal remote sensing identification method of different types of rock desert based on contours, isotherms, and isohyets. This method provides information support for deepening our understanding of the interaction between bare land and soil erosion, and the relationship between the underlying surface of different rock desert and land-atmosphere types. Moreover, it is valuable for the maintenance of the ecological environment and the construction of the Qinghai-Tibet Plateau national park.

## **2 Comparison of types of the rock desert in the ice-snow melting and dry areas**

Rock desert is a type of desert formed by freeze-thaw erosion, wind erosion, gravity erosion, fluvial erosion, and other natural factors, as well as human factors in arid, semi-arid, and dry sub-humid regions. The concrete manifestations include soil coarsening, nutrient and water content tending to decrease, and vegetation coverage and productivity obviously decreasing. Based on the particle size of surface weathered material particles, we can divide the rock desert into bare rock, bare stone, bare gravel, bare sand, and bare soil (Zhao et al., 2019; Jia et al., 2022). According to the different driving forces, we divided the rock desert into the ice-snow melting and dry areas.

### **2.1 Formation mechanism of the two types of rock desert**

The rock desert in both the ice-snow melting and dry areas are the products of climate, but the mechanism is different. The rock desert in the ice-snow melting areas is a bare land formed by the

melting of the covered ice and snow and the retreat of the snow line due to the influence of climate warming on the permanent snow and glaciers in the mountains. The rock desert in the dry areas is a bare land formed due to the lack of precipitation, which cannot meet the minimum precipitation required for vegetation growth. The rock desert in the ice-snow melting areas is affected by climate warming, which changes the land cover from ice and snow to bare land. The rock desert in the dry areas is a bare land formed by precipitation stress. Furthermore, the soil erosion dynamics of the two types of rock desert are different, the rock desert in the ice-snow melting areas is the result of the combined action of freeze-thaw, gravity, wind, and fluvial erosion, while that in the dry areas is primarily caused by the wind erosion of drying denudation.

## 2.2 Differences in material composition and spatial distribution characteristics of the two types of rock desert

### 2.2.1 Rock desert in the ice-snow melting areas

The material composition of the rock desert in the ice-snow melting areas includes bare rock, bare stone, bare gravel, bare sand, and bare soil, and various types are distributed in a staggered manner, among which bare rock and bare stone are the main ones, as shown in Figure 1.

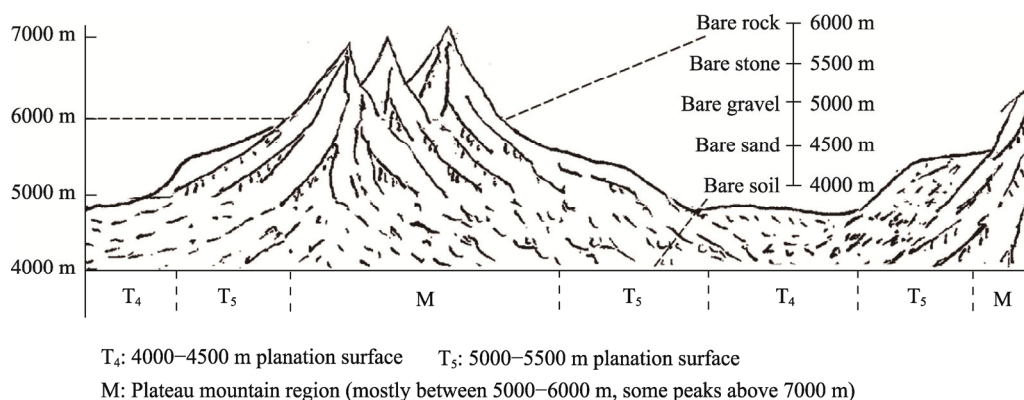


**Fig. 1** Material composition and spatial distribution characteristics of the rock desert in the ice-snow melting areas (hand-painted by Prof. SHI Peijun)

Based on the material composition and spatial distribution characteristics of the rock desert in a typical ice-snow melting area, Prof. SHI Peijun hand-painted Figure 1 during the Second Qinghai-Tibet Plateau Scientific Expedition and Research on 28 July 2021. The area in Figure 1 is located at the junction of Maqen Country and Jigzhi Country in Golog Tibetan Autonomous Prefecture, Qinghai Province of China, in the hinterland of the Qinghai-Tibet Plateau. On the vertical gradient transition, the geomorphic types from the foothills to the top of the mountain change from the 4000–4500 m planation surface (T<sub>4</sub>) and the 5000–5500 m planation surface (T<sub>5</sub>) to the plateau mountain region which is mostly between 5000–6000 m (M) with the increase of elevation. The types of rock desert are in the elevation range of 4000–6000 m, with bare soil, bare sand, bare gravel, bare stone, and bare rock from bottom to top, and are covered with ice and snow above 6000 m. Owing to the wide distribution of the ice-snow melting areas on the Qinghai-Tibet Plateau, the geographical environment of each region is different, the distribution types of vertical gradients of rock desert in different regions are not as complete as the five types of rock desert shown in Figure 1. Moreover, the elevation range fluctuates between 4000 and 6000 m.

### 2.2.2 Rock desert in the dry areas

Compared with the rock desert in the ice-snow melting areas, there are obvious differences in the material composition and spatial distribution of that in the dry areas. The material composition of rock desert in the dry areas also includes bare rock, bare stone, bare gravel, bare sand, and bare soil. Rock desert in the dry areas is distributed horizontally and in patches, primarily in inland basins and on both sides of river valleys in the dry areas, as shown in Figure 2.

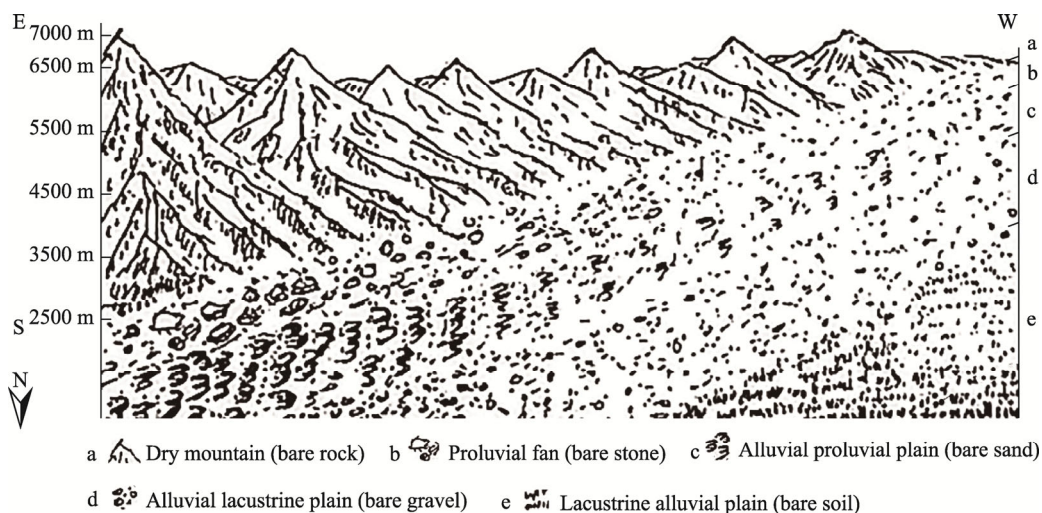


**Fig. 2** Material composition and spatial distribution characteristics of rock desert in the dry areas (hand-painted by Prof. SHI Peijun). The mountains are located on the southern side of the valley plain, the direction of the mountains is east-west.

Prof. SHI Peijun hand-painted Figure 2 in the Qaidam Basin in the northern Qinghai-Tibet Plateau on 31 July 2021, based on the material composition and spatial distribution characteristics of the rock desert in a typical dry area. Within the scope of Figure 2, the geomorphic types transition from the foot of the mountain to the top of the mountain, as well as from piedmont plain and diluvial fan to dry mountain. Bare rock is only distributed in the dry mountain area with large slope, bare stone is primarily distributed in the proluvial fan area under the dry mountain area, while bare sand, bare gravel, and bare soil are distributed in the alluvial proluvial plain and lacustrine alluvial plain. The Qaidam Basin primarily contains a vast gobi, and the distribution of the dry mountain areas and piedmont alluvial fans is small; therefore, the distribution area of bare rock and bare stone is small. Bare gravel is distributed on both sides of the river valley in the dry areas, while bare sand and bare soil are distributed in a wide basin.

### 3 Materials and methods

#### 3.1 Study area and data collection

##### 3.1.1 Study area

The study area ( $35^{\circ}21' - 37^{\circ}39'N$ ,  $93^{\circ}25' - 96^{\circ}15'E$ ) is located in the northern part of the Qinghai-Tibet Plateau, centered on Yuzhu Peak, the highest peak in the eastern Kunlun Mountains, with a total area of  $6.2 \times 10^4 \text{ km}^2$ . The study area includes the west of the Nomhon River, the southeast of Dong Taijnar Lake, and the northwest of the Sonam Darjee Conservation Station. (Fig. 3). The Kunlun Mountains lie across this area, with the Qaidam Basin in the north and Yushu Plateau in the south. The Qaidam Basin is an arid area with scarce precipitation (average annual precipitation less than 100 mm), and the terrain is flat; Yushu Plateau has permafrost and typical periglacial geomorphic characteristics. The climate is a typical plateau alpine climate with large topographic fluctuations. Because of the obvious differences in climate and geomorphology between the north and the south, the unique geographical location, strong winds, abundant sand sources, and cold and dry climate all provide favorable conditions for the occurrence of rock desert in the plateau. Therefore, the region has a good regional representation and is an ideal region for the study of the rock desert in the ice-snow melting and dry areas.

##### 3.1.2 Data collection and image preprocessing

The data used in this study include: (1) Landsat8 OLI image data; the Path/Row numbers are P136R034, P136R035, P137R034, and P137R035, and the imaging times are 30 August 2020, 15



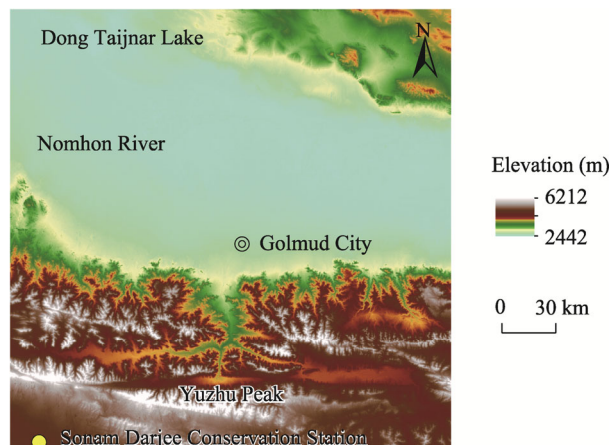


**Fig. 3** Overview of the study area

September 2020, 22 September 2020, and 22 September 2020, respectively. The spatial resolution is 30 m×30 m, and the cloud cover is less than 10%, obtained from the United States Geological Survey (USGS) website (<http://glovis.usgs.gov/>); (2) Advanced Spaceborne Thermal Emission and Reflection Radiometer Global Digital Elevation Model (ASTER GDEM), which is produced in October 2011. There are 12 digital elevation models covering the study area, and their data numbers range from N35E093–N35E096, N36E093–N36E096, and N37E093–N37E096. The spatial resolution is 30 m×30 m, which is set by the Website of China Geospatial Data Cloud (<https://www.gscloud.cn/>); and (3) temperature and precipitation raster data; the data are collected from the National Qinghai-Tibet Plateau Scientific Data Center (<http://data.tpdc.ac.cn/>) during January 1991–December 2018 with the spatial resolution of 1 km×1 km (He et al., 2020).

Image preprocessing includes geometric correction, radiometric calibration, atmospheric correction, terrain correction, and projection transformation. Geometric correction eliminates the geo-metric error in remote sensing images, and makes the same ground object appear in the same position of the corrected image; radiation calibration converts the digital number value of a pixel into radiance to obtain the reflectivity of the top of the atmosphere; atmospheric correction eliminates the influence of atmospheric absorption and scattering on the real reflectivity of ground objects; terrain correction eliminates the influence of complex terrain on radiance to obtain the real reflectivity of ground objects. Finally, the projections of OLI image, DEM data, and temperature and precipitation raster data are converted into the Albers equal area cone projection.

### 3.2 Contour extraction of terrain

DEM is a dataset that realizes the digital simulation of ground terrain through limited surface elevation information and describes ground elevation information through regular grid points within a certain range. DEM is used to reflect the spatial distribution of regional geomorphology, and it is the approximate description of terrain used for determining a comprehensive scale (Li et al., 2018). Contour, as the most effective expression of three-dimensional topography on a two-dimensional plane, can reflect the situation of surface fluctuation and the characteristics of surface morphology (Wang et al., 2018). Contour refers to the closed curve connected by adjacent points with equal elevation on a topographic map (Wang et al., 2021). Although contours are closed curves in theory, in fact, owing to the limitation of the map frame, we can divide contours into closed curves in the map and open curves with two endpoints on the map frame boundary.

In the study area, the lowest elevation is 2442 m, the highest elevation is 6212 m, and the relative ground fluctuation is 3770 m. In the mountain areas, a large slope and complex surface fragmentation are found. In general, the temperature decreases by 0.6°C for every 100 m. Therefore, in order to effectively connect topographic and meteorological elements, we select a vertical

interval to extract contour lines at 100 m intervals. Contour extraction is based on ArcGIS 10.5. The contour tool from the software uses regular grid DEM as the data source to generate contours.

### 3.3 Extraction of isotherms and isohyets

Temperature and precipitation are the basic elements of climate change. To a certain extent, they reflect the dry and wet conditions of the region and are important indicators of the natural division between dry and wet areas. They are both important climatic factors that affect the spatial distribution of rock desert types (Xu et al., 2009). Climatic characteristic lines (isotherms and isohyets) are important reference indices for natural zoning and can be used as effective dividing lines for the distribution range of the rock desert in the ice-snow melting and dry areas formed by climate.

The realization process of isotherms and isohyets is as follows. Firstly, annual average temperature and average annual precipitation are calculated through meteorological data for several years. Because the meteorological data format is separated month by month, the amount of data is large; therefore, the code processing is written based on the MATLAB (Version R2019a) platform to achieve the following two goals: (1) the monthly average temperature data from 1991 to 2018 were averaged as annual average temperature, and the multi-year mean temperature was calculated based on these data; and (2) the monthly precipitation data from 1991 to 2018 were accumulated into annual precipitation, and the average annual precipitation was calculated based on these data. The mean temperature and precipitation raster TIFF data with the required time resolution are obtained. Secondly, based on ArcGIS 10.5 software, we used tools such as reclassification and raster-vector conversion to extract the isohyets in 10 mm intervals and isotherms in 1°C intervals in the study area.

### 3.4 Two types of rock desert areas remote sensing identification based on multi-element overlay analysis

Through multi-source data compounding, we identified the bare areas based on the NDVI method, and adopted the multi-element fusion of contours, isotherms, and isohyets to efficiently implement the extraction process of the two types of rock desert areas with high precision (Fig. 4).

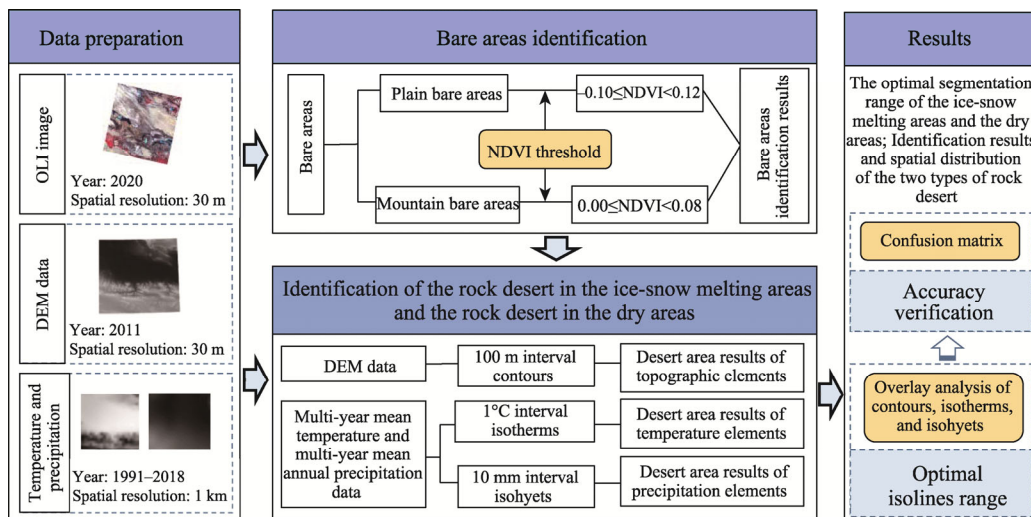


**Fig. 4** Remote sensing identification process of the rock desert in the ice-snow melting and dry areas. OLI, operational landscape imager; DEM, digital elevation model.

#### 3.4.1 Identification of the bare areas based on the normalized difference vegetation index (NDVI)

The main geomorphic types in the study area include the mountain and plain areas, among which P136R035 and P137R035 are mostly the mountain areas, and P136R034 and P137R034 are the

plain areas (Fig. 5). There are various types of land use in the mountain areas, including vegetation, bare land, water, residential land, and ice-snow covered land. The spatial distribution for these land types has no obvious characteristics, and the land types are relatively fragmented. The bare land in the areas is primarily caused by the melting of ice and snow, which is distributed in the ice-snow melting areas, and it is small and patchy. The land use types in the plain areas include vegetation, bare land, water, residential, and industrial land. The bare land in the areas is primarily caused by drought, and it is large and distributed in patches.

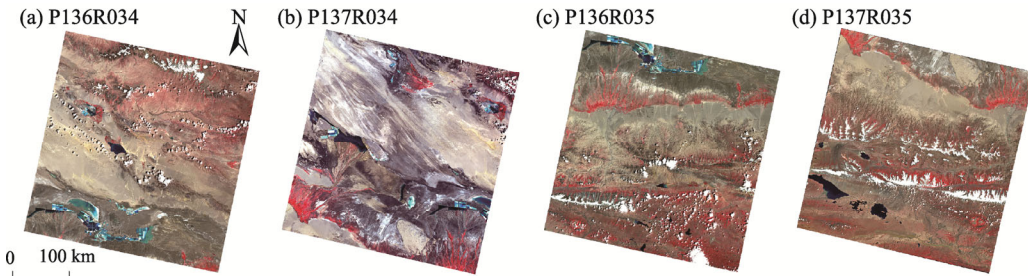


**Fig. 5** Landsat8 OLI images of the study area. (a and b), the images of plain areas; (c and d), the images of mountain areas. P136R034, P137R034, P136R035, and P137R035 are the path/row numbers of the remote sensing image used.

The bare and non-bare areas have different material compositions and geomorphology types, and the vegetation coverage in the bare areas is lower than that in the non-bare areas. The NDVI is the most widely used index to reflect the vegetation coverage, and it is an important distinguishing factor between the bare areas and the non-bare areas (Eisfeld et al., 2012). The NDVI is the most efficient method of all vegetation and drought indices in the bare areas (Higginbottom et al., 2014). The calculation formula of NDVI is as follows:

$$\text{NDVI} = (\text{NIR} - \text{RED}) / (\text{NIR} + \text{RED}), \quad (1)$$

where RED and NIR are the reflectance values of the red band and near infrared band, respectively, with values ranging from  $-1$  to  $1$ . Generally, the NDVI less than zero indicates a non-vegetation area, and the NDVI greater than zero represents a vegetation area. To effectively determine the NDVI thresholds for bare and non-bare areas, we divided the image into  $1 \text{ km} \times 1 \text{ km}$  grids using the fishnet tool, extracted the NDVI value of the center point of each grid, and counted the threshold range of NDVI for land use types in the mountain and plain areas (Table 1). Finally, the NDVI threshold of the bare areas is determined as follows:  $-0.10$ – $-0.12$  in the plain areas and  $0.00$ – $0.08$  in the mountain areas.

**Table 1** Normalized difference vegetation index (NDVI) threshold of each land use type in the bare areas

Plain areas		Mountain areas	
Land use type	NDVI threshold	Land use type	NDVI threshold
Water, residential land, and industrial land	$\leq -0.10$	Water, residential land	$\leq -0.10$
Bare land	$-0.10$ – $-0.12$	Ice-snow covered land	$-0.10$ – $0.00$
Vegetation	$\geq 0.12$	Bare land	$0.00$ – $0.08$
		Vegetation	$\geq 0.08$

### 3.4.2 Identification of the two types of rock desert areas by considering topographic and meteorological elements

Based on the formation mechanism of the two types of rock desert areas, the spatial distribution is determined by elevation, temperature, and precipitation. Therefore, for the identification results of the bare areas, the contour results from the topographic elements are overlain with



OLI images in the study area to determine the optimal segmentation contour of the rock desert in the ice-snow melting and dry areas. According to the isoline element overlay analysis method, we superposed and analyzed the best divided contours, isotherms, and isohyets, and determined the ranges of isotherms and isohyets that are closest to the optimal contour distribution. Finally, the contour results of the topographic elements, and the isotherms and isohyets results of meteorological elements are obtained. The combination of three isoline ranges is the optimal combination of dividing lines in the identification of the rock desert in the ice-snow melting and dry areas.

### 3.5 Accuracy verification method

The evaluation of identification results is an important part of remote sensing monitoring, and it is also a measure of the reliability of identification results. Accuracy verification determines the accuracy of the processing process by comparing actual data with processed data. The most commonly used verification method is the confusion matrix method, which is calculated by comparing the position and category of each measured pixel with the corresponding position and category in the identification results (Kong et al., 2012). Each column of the confusion matrix represents the actual measured information, and the value in each column is equal to the number of actually measured pixels corresponding to the corresponding category in the identification results; each row of the confusion matrix represents the information of the identification results, and the value in each row is equal to the number of identification results pixels in the corresponding category of the measured pixels. The accuracy of identification results can be comprehensively reflected by using confusion matrix (McCallum et al., 2006).

To verify the accuracy of remote sensing identification, we used global positioning system (GPS) field sampling in the study area from 24 September to 29 September in 2021. Based on the principle of traffic accessibility, we took the sampling points from the bare areas, the non-bare areas, the rock desert in the dry areas, the rock desert in the ice-snow melting areas, and the transition area. Each sampling point was located by GPS, and the geographic coordinates, elevation, land use type, and vegetation coverage of the sampling point were recorded; a total of 248 sampling points were obtained.

## 4 Processes and results

### 4.1 Accuracy verification

#### 4.1.1 Accuracy verification of the bare areas identification

A total of 139 sampling points in the bare areas and 109 sampling points in the non-bare areas were collected by GPS. In the plain areas, there are 92 sampling points in the bare areas and 40 sampling points in the non-bare areas (primarily vegetation); in the mountain areas, the bare areas are primarily distributed in the ice-snow melting areas, which are difficult to reach, and a total of 47 samples were collected, while 69 samples are collected in the non-bare areas (primarily vegetation and a small amount of ice-snow covered areas). The accuracy verification results of the plain, mountain, and whole study areas based on the confusion matrix are shown in Table 2.

Table 2 shows that the identification accuracy of the bare areas based on the NDVI method is better, with an overall accuracy of 93.95% and Kappa coefficient of 0.88. The identification accuracy of the plain areas is better than that of the mountain areas. There are less land types in the plain areas, and the bare areas are distributed in patches; thus, the identification accuracy is high, and Kappa coefficient can reach 0.91. However, the bare areas in the mountain areas are mostly caused by the melting of ice-snow and distributed in the ice-snow melting areas; the pattern spots are broken. The identification accuracy in the mountain areas is slightly lower than that in the plain areas, but Kappa coefficient can still reach 0.82, which can meet the other requirements in this study.

**Table 2** Accuracy verification results of the bare areas identification

Type		Producer's accuracy (pixel)	User's accuracy (pixel)	Producer's accuracy (%)	User's accuracy (%)	Overall accuracy (%)	Kappa coefficient
Plain areas	Bare areas	90/92	90/93	97.83	96.78	96.21	0.91
	Non-bare areas	37/40	37/39	92.50	94.87		
Mountain areas	Bare areas	41/47	41/45	87.23	91.11	91.38	0.82
	Non-bare areas	65/69	65/71	94.20	91.55		
Whole study areas	Bare areas	131/139	131/138	94.24	94.93	93.95	0.88
	Non-bare areas	102/109	102/110	93.58	92.73		

Note: The fractions are used in the column of Producer's accuracy and User's accuracy, where the numerator represents the number of grids of each rock desert category in the verified sample and the denominator means the number of grids of each rock desert category actually calculated.

#### 4.1.2 Accuracy verification of identification of rock desert in the ice-snow melting and dry areas and transition area

The results of rock desert in the ice-snow melting and dry areas are identified by using remote sensing integrated contours, isotherms, and isohyets. A total of 139 sampling points in the bare areas were collected by GPS, with 42 sampling points in the ice-snow melting areas, 88 sampling points in the dry areas, and 9 sampling points in the transition area. The accuracy verification results of identification of rock desert in the ice-snow melting and dry areas and transition area based on the confusion matrix are shown in Table 3.

**Table 3** Accuracy verification results of identification of rock desert in the ice-snow melting and dry areas and transition area

Type	Producer's accuracy (Pixel)	User's accuracy (Pixel)	Producer's accuracy (%)	User's accuracy (%)	Overall accuracy (%)	Kappa coefficient
Rock desert in the ice-snow melting areas	36/42	36/43	85.71	83.72	88.45	0.77
Rock desert in the dry areas	80/88	80/86	90.91	93.02		
Transition area	7/9	7/10	77.78	70.00		

Note: The fractions are used in the column of Producer's accuracy and User's accuracy, where the numerator represents the number of grids of each rock desert category in the verified sample and the denominator means the number of grids of each rock desert category actually calculated.

Table 3 shows that the combination of dividing line ranges from integrating contours, isotherms, and isohyets has better identification accuracy for the rock desert in the ice-snow melting and dry areas, with an overall accuracy of 88.45% and Kappa coefficient of 0.77. The identification accuracy of the rock desert in the dry areas is better than that in the ice-snow melting areas. The identification accuracy of the transition area is relatively low, as the transition area is located in the middle of the two types of rock desert areas, and the probability that the rock desert in the ice-snow melting and dry areas are wrongly divided into the transition area is high. Moreover, it may be related to the small number of sampling points in the transition area. The dividing line considers not only the topographic factors that have significant influence on the spatial distribution of the two types of rock desert areas, but also the meteorological factors. It can provide a scientific reference for the effective identification of the two types of rock desert areas.

#### 4.2 Remote sensing identification results of the bare areas

The NDVI results are calculated using Landsat8 OLI remote sensing images with similar sampling times in 2020 (Fig. 6). Based on the calculation results, the NDVI results of the plain areas (Fig. 6a and b) include three colors, white is vegetation, black is water, residential land, and industrial land, and gray is bare area. The NDVI results of the mountain areas (Fig. 6c and d) have more colors, among which, white and light gray are vegetation, black is water, residential land, and industrial land, dark gray is ice-snow covered area, and medium gray is bare area.

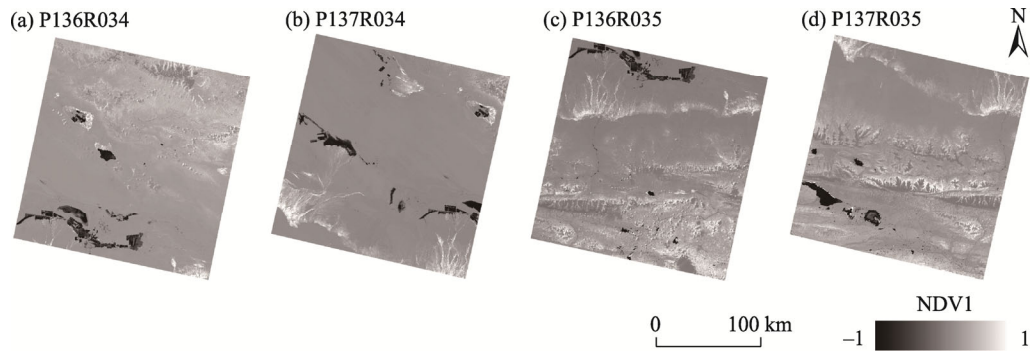


**Fig. 6** Calculation results of the NDVI based on OLI images. (a and b), the images in the plain areas; (c and d), the images in the mountain areas. P136R034, P137R034, P136R035, and P137R035 are the Path/Row numbers of the remote sensing image used.

Based on the statistical results of the NDVI threshold of typical sampling points, the NDVI threshold range in the plain bare areas is slightly wider than that in the mountain bare areas. The wider the spatial distribution of the bare areas, the larger the NDVI threshold range; conversely, the more land types, the smaller the spatial distribution range, and the more concentrated the NDVI threshold range. The extent of the bare areas determined based on the NDVI method is shown in Figure 7. The total area of the bare areas is  $3.72 \times 10^4 \text{ km}^2$ , accounting for 60.00% of the study area.

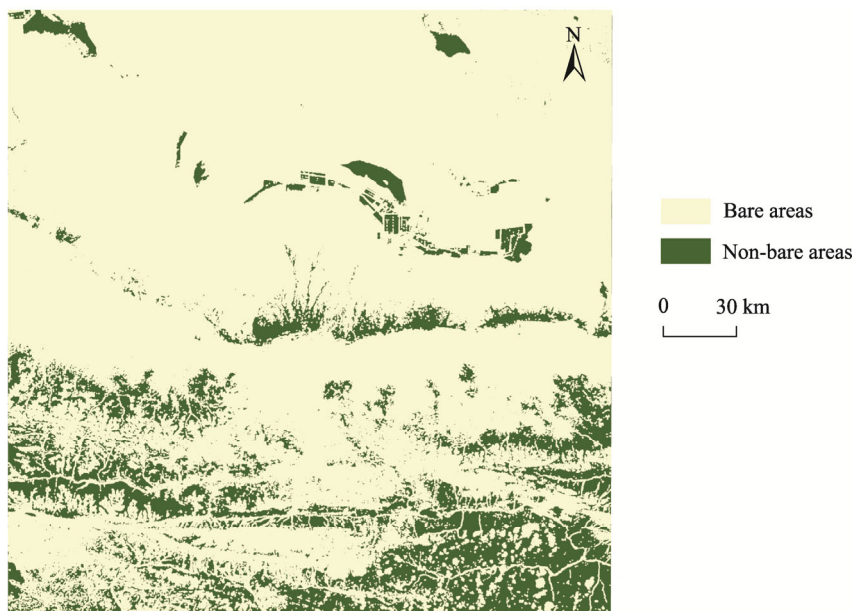


**Fig. 7** Identification results of the bare areas based on the NDVI method

#### 4.3 Remote sensing identification results of the two types of rock desert areas

The extraction results of 100 m interval contours of DEM data, as well as  $1^\circ\text{C}$  interval isotherms and 10 mm interval isohyets of meteorological data are shown in Figure 8. In the study area, the topography fluctuates greatly, the relative height difference is 3770 m, and the data of contours at intervals of 100 m are still dense, trending low in the north and high in the south. Taking the north Kunlun Mountains as the boundary, the contours in the Qaidam Basin in the north range from 2500 m to 3600 m, concentrated in the elevation range of 2700–3300 m. The Yushu Plateau in the south is between 3600 and 6200 m; from 1991 to 2018, the annual average temperature in the study area was higher in the north and lower in the south. The isotherms in the Qaidam Basin are

between 2°C and 7°C, and those in the Yushu Plateau are between −9°C and 5°C. The average annual precipitation is lower in the north and higher in the south. The isohyets in the Qaidam Basin are between 50 and 100 mm, and those in the Yushu Plateau are between 100 and 240 mm.

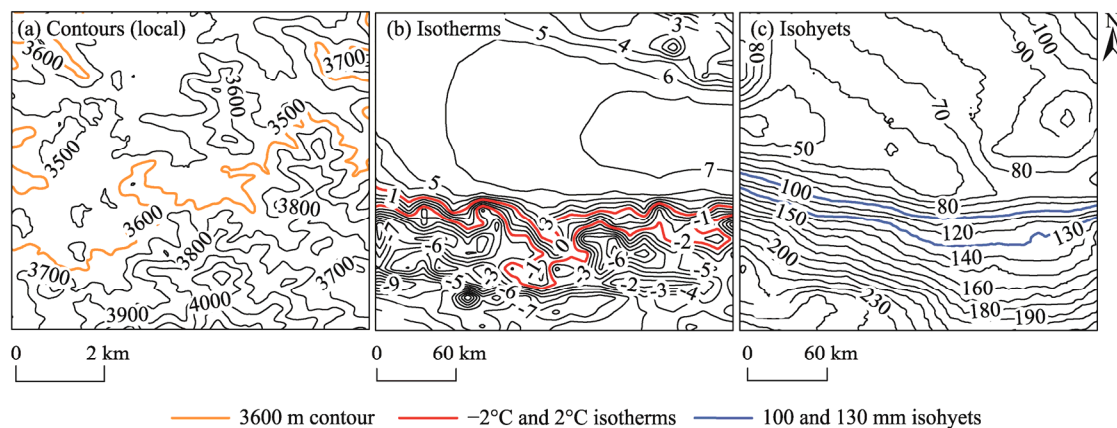


**Fig. 8** Extraction results of contours (a), isotherms (b), and isohyets (c)

Based on the overlay analysis of the contour results for the topographic elements and OLI images in the study area, we determined that the optimal dividing contour of the rock desert in the ice-snow melting and dry areas is 3600 m. Using an overlay of contour elements, we superposed the optimally divided contours with isotherms and isohyets to determine that isotherms and isohyets range closest to the optimal contour distribution. There is an obvious negative correlation between temperature and elevation. The isotherms range of −2°C–2°C is consistent with the contour line of 3600 m; therefore, the isotherms range of −2°C–2°C is set as the dividing line between the two types of rock desert areas. Owing to the influence of southwest monsoon, when the water vapor from the Indian Ocean moves from the south slope of the Kunlun Mountains to the north slope, the isohyets change from dense to sparse at 100–130 mm; thus, the isohyets range of 100–130 mm is set as the dividing line between the two types of rock desert areas (Fig. 9).

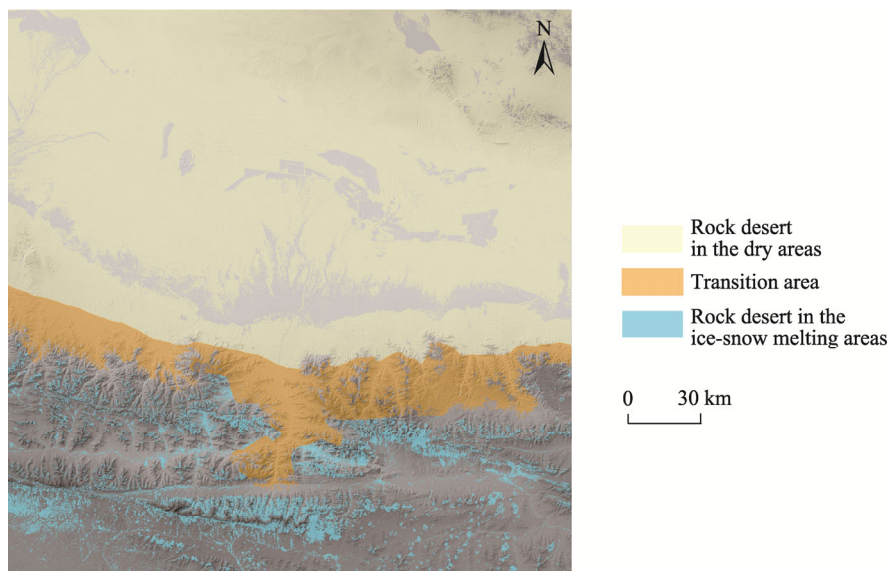


**Fig. 9** Identification results overlay multi-factor analysis for the two types of rock desert areas

Figures 8 and 9 show that the 3600 m contour, the −2°C–2°C isotherms, and the 100–130 mm isohyets are relatively close in space. The 3600 m contour and the −2°C–2°C isotherms are

influenced by the trend of the Kunlun Mountains, and the trend of the two lines is basically the same. The isohyets practically coincide with the isotherms on the east side, and are slightly norther than the isotherms on the west side. This is primarily due to the obvious negative correlation between temperature and elevation, and the decrease of precipitation is also influenced by the gradient and aspect of the windward slope. Thus, in the areas with elevation less than 3600 m, annual average temperature higher than 2°C, and precipitation less than 100 mm are regarded as the rock desert in the dry areas. The range of −2°C–2°C isotherms and 100–130 mm isohyets is the transition area between the two types of rock desert areas. The areas with elevation higher than 3600 m, annual average temperature less than −2°C, and average annual precipitation higher than 130 mm are the rock desert in the ice-snow melting areas. The rock desert in the dry areas covers a total of  $3.14 \times 10^4$  km<sup>2</sup>, accounting for 84.40% of the bare areas. The rock desert in the ice-snow melting areas covers a total of  $0.34 \times 10^4$  km<sup>2</sup>, accounting for 9.14% of the bare areas. The transition area between the two types of rock desert areas covers a total of  $0.24 \times 10^4$  km<sup>2</sup>, accounting for 6.46% of the bare areas.

## 5 Discussion

### 5.1 Applicability evaluation of identification of the bare areas based on the NDVI

The bare areas in the study region primarily includes plain and mountain bare areas. The spatial distribution range and number of land types of the two bare areas are quite different, and the identification accuracy is also different. The segmentation results of different land class densities in the plain and mountain areas based on the NDVI are shown in Figures 10 and 11.

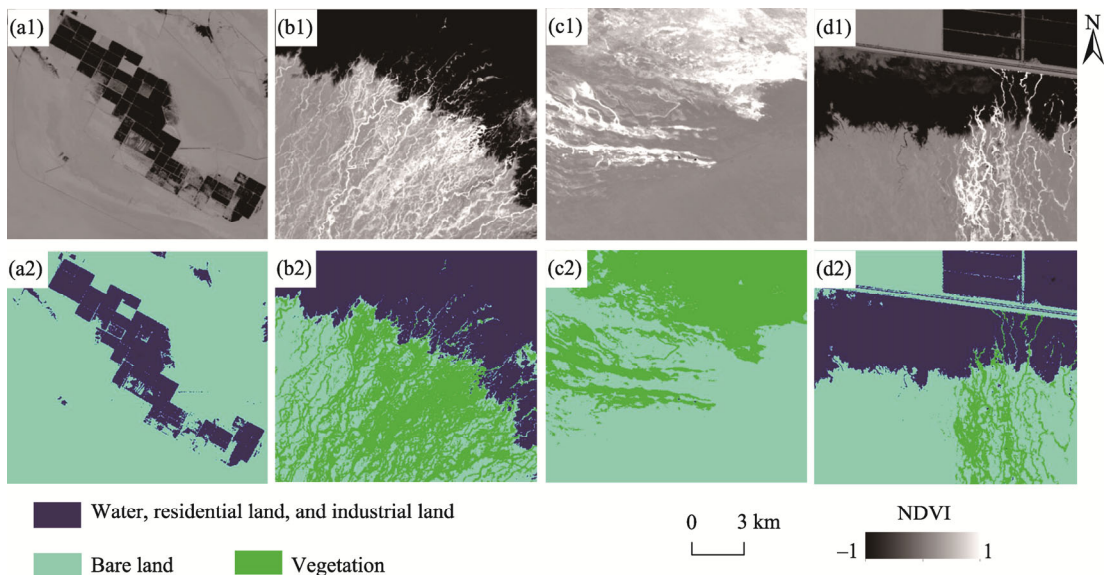


**Fig. 10** NDVI (a1–d1) and NDVI density segmentation (a2–d2) results in the plain areas

The plain areas were primarily located in the dry Qaidam Basin, and the land type is the bare land, with a small proportion of water, residential land, industrial land, and vegetation. The spatial distribution of each type is highly heterogeneous, and the contiguous distribution characteristics of the bare land is obvious. Figure 10 shows that the segmentation effect of the bare areas and other land types (water, residential land, industrial land, vegetation) is good. The boundary of residential land and industrial land (Fig. 10a1 and a2) and water (Fig. 10b1 and b2) is clear, and the boundary between vegetation (Fig. 10c1 and c2) and bare area is clearly demarcated. Furthermore, roads (Fig. 10d1 and d2) and water in residential land and industrial land can be well identified. Therefore, the NDVI has high applicability to the dry bare land in the plain areas.



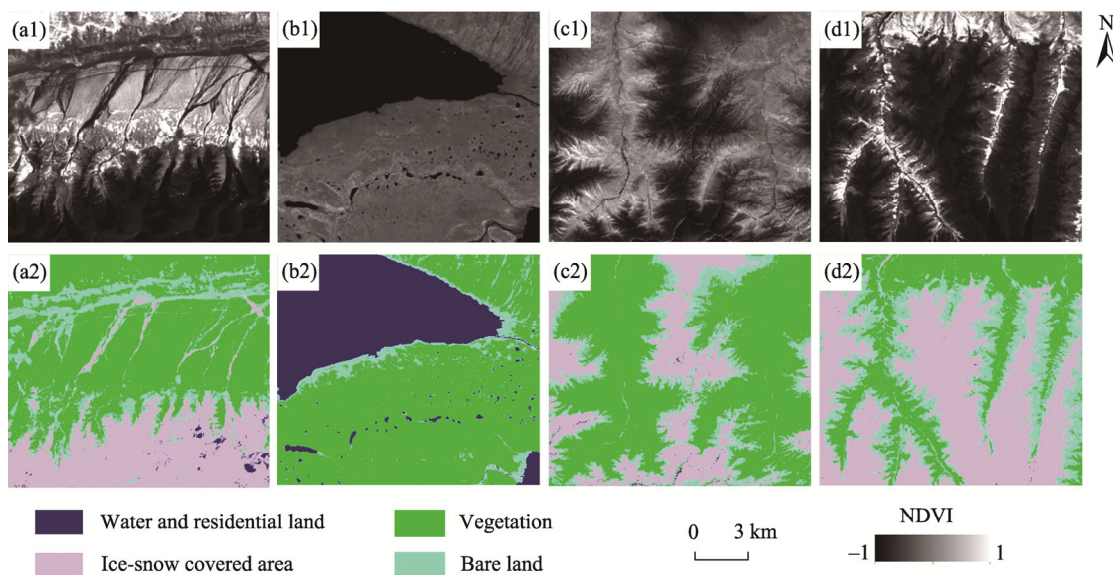


**Fig. 11** NDVI (a1–d1) and NDVI density segmentation (a2–d2) results in the mountain areas

Most of the mountain areas are located on the Yushu Plateau, and the land type is primarily vegetation, and the bare land is typically distributed in the ice-snow melting areas in the high mountains, with a small proportion and fragmented patterns. Figure 11 shows that the bare areas can be distinguished from the ice-snow covered areas (Fig. 11c1 and c2) and vegetation (Fig. 11d1 and d2) well, but a small number of rivers will be wrongly classified into vegetation. In the extremely high mountain areas (i.e., the Yuzhu Peak; Fig. 11a1 and a2), the discrimination of various types is poor, and the ice-snow covered areas are wrongly divided into the water areas, and the bare land and water are partially misclassified. For the bare land around a large area of water (Fig. 11b1 and b2), the discrimination is high. The identification effect of the NDVI on the bare land in the mountain areas is slightly lower than that on the dry bare land in the plain areas, the accuracy evaluation of the bare areas can also verify this result, but it can also provide support for rapid and efficient monitoring of the bare areas in the mountain areas. In conclusion, the identification of the bare areas based on the NDVI has good applicability. To further improve the identification accuracy of the bare land in the mountain areas, the combination of multi-index or multi-indicator can be considered in the future.

## 5.2 Uncertainty evaluation of isoline combination results

The identification results of the rock desert in the ice-snow melting and dry areas are isotherms and isohyets obtained from the meteorological grid data from 1991 to 2018. To further explore the uncertainty of the isoline combination results, we drew the trend chart of the annual average temperature and average annual precipitation from 1991 to 2018 (Fig. 12).

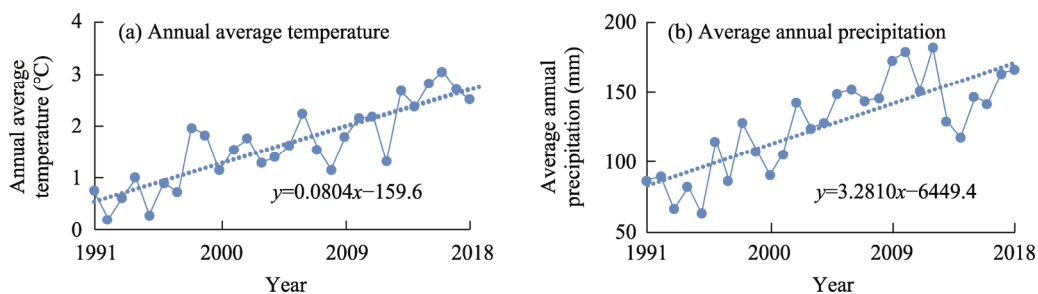


**Fig. 12** Variation trend of annual average temperature (a) and average annual precipitation (b) from 1991 to 2018

According to the variation trend of annual average temperature and average annual precipitation in the study area from 1991 to 2018 in Figure 11, we can conclude that the temperature is rising at a rate of  $0.8^{\circ}\text{C}/10\text{ a}$ , and the precipitation is rising at a rate of  $32.8\text{ mm}/10\text{ a}$ . With the further change of temperature and precipitation in the future, the isotherms and isohyets are expected to migrate, changing the optimal dividing line combination between the ice-snow melting and dry areas. In recent years, the eastern part of Kunlun Mountains has shown the same trend of warming and humidification as the Qinghai-Tibet Plateau. With the change of temperature and precipitation, the range of isotherms and isohyets fluctuates. The increase of temperature in the study area leads to the increase of isotherms value, and the increase of precipitation leads to the increase of isohyets value. Isotherms and isohyets within the isoline combination are expected to increase, and at the same time, the range of the two types of rock desert areas will change slightly.

### 5.3 Uncertainty of rock desert classification system

The classification of desert types is a process of merging groups according to the similarity and difference of desert land. According to the external forces and causes, we divided the desert into wind-eroded desert, water-eroded desert, freeze-thaw desert, and land salinization; according to climate type, we divided the desert into arid desert, semi-arid desert, and sub-humid desert; according to the development degree of desert, we divided the desert into mild desertification, moderate desertification, and severe desertification; according to the particle size of surface composition, we divided the desert into stony desert, gravel desert, sandy desert, and salt desert, etc. (Cristina and Abigai, 2017; Javier et al., 2018; Çağlar and Orhan, 2020). Taking climate zoning as the main indicator, combined with external forces as well as current land use and surface characteristics of degraded land, the Qinghai-Tibet Plateau desert can be divided into arid desert and freeze-thaw desert (Wang and Sun, 1996; Li et al., 2005). And freeze-thaw desert includes rock desert in ice-snow melting areas (Jia et al., 2022).

In this paper, the types of rock desert on the Qinghai-Tibet Plateau are divided into rock desert in the ice-snow melting areas and rock desert in the dry areas, which is helpful to distinguish the rock desert from the formation mechanism. According to the results of field investigation in the study area, we divided the rock desert into bare rock, bare stone, bare gravel, bare sand, and bare soil based on the particle size of surface weathered material particles, this consideration is only limited to the scope of the study area. The rock desert in the ice-snow melting areas is primarily bare rock and bare stone, while the rock desert in the dry areas is mainly bare gravel, bare sand, and bare soil. In contrast, the grain size of the weathered rock desert in the ice-snow melting areas is larger than that in the dry areas, because the rock desert in the ice-snow melting areas has only been exposed to the surface in recent decades, and the weathering degree is lower than that in the dry areas. However, the rock desert in the dry areas is affected by the long-term combined erosion of wind, water, gravity, and freeze-thaw; thus, the particle size of weathered material is relatively small. There are obvious differences in the physical and geographical characteristics of the various regions within the Qinghai-Tibet Plateau, and the specific classification types should be further rationally divided according to the specific material composition structure of the regional rock desert.

## 6 Conclusions

(1) The multi-element fusion method of contours, isotherms, and isohyets can effectively identify the rock desert in the ice-snow melting and dry areas. The accuracy verification results for the identification of rock desert areas based on the fusion of contours, isotherms, and isohyets show that the accuracy based on multi-factor identification is high, with an overall accuracy of 88.45% and kappa coefficient of 0.77. The identification method not only considers the topographic factors that have significant influence on the spatial distribution of the two types of rock desert areas, but also the meteorological factors, providing a scientific reference for the effective

identification of the two types of rock desert areas.

(2) The optimal dividing range of the rock desert in the ice-snow melting and in dry areas are the 3600 m contour,  $-2^{\circ}\text{C}$ – $2^{\circ}\text{C}$  isotherms, and 100–130 mm isohyets. Based on the identification result from multi-factor fusion method of contours, isotherms, and isohyets, the area with elevation less than 3600 m, annual average temperature higher than  $2^{\circ}\text{C}$ , and average annual precipitation less than 100 mm is rock desert in the dry areas. The range of the  $-2^{\circ}\text{C}$ – $2^{\circ}\text{C}$  isotherms and 100–130 mm isohyets is the transition area between the two types of rock desert areas. The area with elevation higher than 3600 m, annual average temperature less than  $-2^{\circ}\text{C}$ , and average annual precipitation higher than 130 mm is the rock desert in the ice-snow melting areas.

(3) The identification accuracy of plain bare areas is better than that of mountain bare areas based on the NDVI. There are few land types in the plain areas, and the bare areas are widely distributed in patches. The bare areas of the mountain areas are primarily caused by the melting of ice-snow and distributed in the ice-snow melting areas, with small and broken patches. The NDVI threshold range of plain bare areas is  $-0.10$  to  $0.12$ , which is slightly wider than that of mountain bare areas ( $0.00$  to  $0.08$ ). The bare areas cover  $3.72 \times 10^4 \text{ km}^2$ , accounting for 60.00% of the study area.

## Acknowledgements

This research was funded by the Natural Science Foundation of Qinghai Province of China (2021-ZJ-905) and the Second Qinghai-Tibet Plateau Scientific Expedition and Research Program of China (2019QZKK0606). We thank the NASA Earth Data Open Access for Open Science.

## References

- Böhner J. 2006. General climatic controls and topoclimatic variations in central and high Asia. *Boreas*, 35(2): 279–295.
- Çağlar Uzuner, Orhan Dengiz. 2020. Desertification risk assessment in Turkey based on environmentally sensitive areas. *Ecological Indicators*, 114: 106295, doi: 10.1016/j.ecolind.2020.106295.
- Chang X L, Jin H J, He R X, et al. 2017. Evolution and changes of permafrost on the Qinghai-Tibet Plateau during the late quaternary. *Sciences in Cold and Arid Regions*, 9(1): 1–19. (in Chinese)
- Cristina N M, Abigail M S V. 2017. Assessing the progress of desertification of the southern edge of Chihuahuan Desert: A case study of San Luis Potosi Plateau. *Journal of Geographical Sciences*, 27(3): 420–438.
- Dawelbait M, Morari F. 2012. Monitoring desertification in a Savannah region in Sudan using Landsat images and spectral mixture analysis. *Journal of Arid Environments*, 80: 45–55.
- Eisfelder C, Kuenzer C, Dech S. 2012. Derivation of biomass information for semi-arid areas using remote-sensing data. *International Journal of Remote Sensing*, 33: 2937–2984.
- Gevaert A I, Miralles D G, de Jeu R A M, et al. 2017. Soil moisture-temperature coupling in a set of land surface models. *Journal of Geophysical Research: Atmospheres*, 123: 1481–1498.
- Guo B, Wei C X, Yu Y, et al. 2021. The dominant influencing factors of desertification changes in the source region of Yellow River: Climate change or human activity? *Science of the Total Environment*, 813(2): 152512, doi: 10.1016/j.scitotenv.2021.152512.
- Han J, Wang J, Chen L, et al. 2021. Driving factors of desertification in Qaidam Basin, China: An 18-year analysis using the geographic detector model. *Ecological Indicators*, 124: 107404, doi: 10.1016/j.ecolind.2021.107404.
- He J, Yang K, Tang W J, et al. 2020. The first high-resolution meteorological forcing dataset for land process studies over China. *Scientific Data*, 7: 25, doi: 10.1038/s41597-020-0369-y.
- Hendersonsellers A. 1996. Interactions of desertification and climate. *Applied Geography*, 16(3): 257–258.
- Higginbottom T, Symeonakis E. 2014. Assessing land degradation and desertification using vegetation index data: current frameworks and future directions. *Remote Sensing*, 6(10): 9552, doi: 10.3390/rs6109552.
- Hu G Y, Dong Z B, Lu J F, et al. 2015. The developmental trend and influencing factors of aeolian desertification in the Zoige Basin, eastern Qinghai-Tibet Plateau. *Aeolian Research*, 19: 275–281.
- Hu Y F, Han Y P, Zhang Y Z. 2020. Land desertification and its influencing factors in Kazakhstan. *Journal of Arid*

- Environments, 180: 104203, doi: 10.1016/j.jaridenv.2020.104203.
- Hua T, Wang X M, Ci Z, et al. 2012. Responses of desertification to climate change in arid and semiarid regions of China over the past millennium. *Journal of Desert Research*, 32(3): 618–624. (in Chinese)
- Javier T, Silva P, Barbosa A A, et al. 2018. Desertification trends in the Northeast of Brazil over the period 2000–2016. *International Journal of Applied Earth Observation and Geoinformation*, 73: 197–206.
- Jia W, Wang J A, Shi P J, et al. 2021. The progress and prospect of remote sensing monitoring of rocky desert dynamic changes in the ice and snow melting area of the Qinghai-Tibet Plateau. *Journal of Geo-information Science*, 23(10): 1715–1727. (in Chinese)
- Jia W, Ma W D, Shi P J, et al. 2022. Monitoring rock desert formation caused by ice–snow melting in the Qinghai-Tibet Plateau using an optimized remote sensing technique: A case study of Yushu Prefecture. *Remote Sensing*, 14: 570, doi: 10.3390/rs14030570.
- Kang S C, Zhang Q Q, Qian Y, et al. 2019. Linking atmospheric pollution to cryospheric change in the Third Pole Region: current progress and future prospects. *National Science Review*, 4: 796–809.
- Kefi S, Rietkerk M, Alados C L, et al. 2007. Spatial vegetation patterns and imminent desertification in Mediterranean arid ecosystems. *Nature*, 449(7159): 213–217.
- Kong Y H, Jing M L. 2012. Research of the classification method based on confusion matrixes and ensemble learning. *Computer Engineering & Science*, 34: 111–117. (in Chinese)
- Lamchin M, Lee J, Lee W, et al. 2016. Assessment of land cover change and desertification using remote sensing technology in a local region of Mongolia. *Advances in Space Research*, 57(1): 64–77.
- Li C, Zhao S S, Wang Q, et al. 2018. Uncertainty modeling and analysis of surface area calculation based on a regular grid digital elevation model (DEM). *International Journal of Geographical Information Science*, 32(2): 1–23.
- Li H, Fu C, Guo W, et al. 2015. Study of energy partitioning and its feedback on the microclimate over different surfaces in an arid zone. *Acta Physica Sinica*, 64(5): 438–451. (in Chinese)
- Li Q, Zhang C L, Shen Y P, et al. 2016. Quantitative assessment of the relative roles of climate change and human activities in desertification processes on the Qinghai-Tibetan Plateau based on net primary productivity. *CATENA*, 147: 789–796.
- Li Q, Zhang C L, Zhou N, et al. 2018. Spatial distribution of aeolian desertification on the Qinghai-Tibetan Plateau. *Journal of Desert Research*, 38(4): 690–700. (in Chinese)
- Li S, Gao S Y, Yang P, et al. 2005. Some problems of freeze-thaw desertification in the Tibetan Plateau: a case study on the desertification regions of the western and northern Plateau. *Journal of Glaciology and Geocryology*, 27(4): 476–485. (in Chinese)
- Liu Y Q, He Q, Zhang H S, et al. 2011. Studies of land-atmosphere interaction parameters in Taklimakan desert hinterland. *Plateau Meteorology*, 30(5): 1294–1299. (in Chinese)
- McCallum I, Obersteiner M, Nilsson S, et al. 2006. A spatial comparison of four satellite derived 1 km Global Land Cover Datasets. *International Journal of Applied Earth Observation and Geoinformation*, 8(4): 246–255.
- Miao L J, Moore J C, Zeng F J, et al. 2015. Footprint of research in desertification management in China. *Land Degradation and Development*, 26(5): 450–457.
- Stauch G. 2015. Geomorphological and palaeoclimate dynamics recorded by the formation of aeolian archives on the Tibetan Plateau. *Earth-Science Reviews*, 150: 393–408.
- Sun J, Hou G, Liu M, et al. 2019. Effects of climatic and grazing changes on desertification of alpine grasslands, Northern Tibet. *Ecological Indicators*, 107: 105647, doi: 10.1016/j.ecolind.2019.105647.
- UNCCD, UNDP. 2012. Climate Change in the African Drylands: Options and Opportunities for Adaptation and Mitigation. [2022-02-25]. [https://franklin.library.upenn.edu/catalog/FRANKLIN\\_9948525673503681](https://franklin.library.upenn.edu/catalog/FRANKLIN_9948525673503681).
- Wang C, Li H, Yang J S, et al. 2015. Study on generation technique of high quality contour lines based on grid DEM. *Journal of Geo-information Science*, 17(2): 160–165. (in Chinese)
- Wang J H, Li S H. 1996. Classification of desertification types and its quantification evaluation system. *Arid Environmental Monitoring*, 10(3): 129–137, 190. (in Chinese)
- Wang R, Yan H, Wang Z. 2021. Hotspots and trends visual analysis of contour automated generalization. *Science of Surveying and Mapping*, 46(10): 167–176, 193. (in Chinese)
- Xie S, Qu J, Zu R, et al. 2013. Effect of sandy sediments produced by the mechanical control of sand deposition on the thermal regime of underlying permafrost along the Qinghai-Tibetan Railway. *Land Degradation and Development*, 24: 453–462.
- Xu Y, Xu C H, Gao X J, et al. 2009. Projected changes in temperature and precipitation extremes over the Yangtze River Basin

- of China in the 21<sup>st</sup> century. *Quaternary International*, 208(1–2): 44–52.
- Yan C Z, Song X, Zhou Y M, et al. 2009. Assessment of aeolian desertification trends from 1975's to 2005's in the watershed of the Longyangxia Reservoir in the upper reaches of China's Yellow River. *Geomorphology*, 112(3–4): 205–211.
- Yang M X, Wang X J, Pang G J, et al. 2019. The Tibetan Plateau cryosphere: Observations and model simulations for current status and recent changes. *Earth-Science Reviews*, 190: 353–369.
- Yao T D, Xue Y K, Chen D L. 2019. Recent Third Pole's rapid warming accompanies cryospheric melt and water cycle intensification and interactions between monsoon and environment: multi-disciplinary approach with observation, modeling and analysis. *Bulletin of the American Meteorological Society*, 100(3): 423–444.
- Zhang C L, Li Q, Shen Y P, et al. 2018. Monitoring of aeolian desertification on the Qinghai-Tibetan Plateau from the 1970s to 2015 using Landsat images. *Science of the Total Environment*, 619: 1648–1659.
- Zhang K C, Qu J J, Han Q J, et al. 2012. Wind energy environments and aeolian sand characteristics along the Qinghai-Tibetan Railway, China. *Sedimentary Geology*, 273–274: 91–96.
- Zhang Z W, Yin H Y, Qian D F, et al. 2019. A preliminary study on the classification system of desert in alpine region—taking Duilongdeqing District as an example. *Journal of Plateau Agriculture*, 3(1): 47–53. (in Chinese)
- Zhao Y Y, Gao G L, Qin S G, et al. 2019. Desertification detection and the evaluation indicators: A review. *Journal of Arid Land Resources and Environment*, 33(5): 81–87. (in Chinese)
- Zu R P, He Z L, Zong Y M, et al. 2014. Review on the influences of sand accumulation on permafrost in the Tibetan Plateau. *Journal of Desert Research*, 34(5): 1208–1214. (in Chinese)